Scattering of Surface Waves By Metallic Obstacles on the Dielectric-Image Line

SAMIR F. MAHMOUD, MEMBER, IEEE, AND JOHN C. BEAL, MEMBER, IEEE

Abstract—**A theoretical treatment of scattering of electromagnetic surface waves from thin metallic obstacles of a semiannular shape on the dielectric-image line is presented.**

The method of treatment relies heavily on the expansion of the total fields of the line in terms of its complete set of discrete and continuous modes which in turn is fully derived.

I. INTRODUCTION

SURFACE-WAVE transmission lines form a general class of open guiding structures that appears to have much potential for the provision of continuous-access guided communication (CAGC) on ground transportation systems such as railways, highways, and monorails. Various experimental and theoretical studies have been performed in recent years; for example, Gallawa *et al.* [1] have reported an extensive investigation of the Goubau line for two-way continuous communications. More recently, Beal *et al.* [2] have given a brief review of the subject with the definition of CAGC extended to include guideway obstacle detection, sometimes referred to as "guided radar."

Even in present railway systems general obstacle detection leaves much to be desired, but for high speed systems of the near future and for automated highways, some more satisfactory method of obstacle detection must be developed. In a guided radar scheme, an obstacle is detected either by the reflected signal on a surface-wave guiding structure installed on the track, or by the transmission loss of signals generated by transponders along the line. The two types of operation are described in detail in [2]–[4] where other references are also listed.

Guideway obstructions can be broadly classified into the following.

1) *Dielectric Obstacles*: These include landslides and snowslides which might be more appropriate to detection by their transmission loss. The scattering problem associated with these obstacles will be treated in a subsequent paper.

2) *Metallic Obstacles*: These are primarily preceding vehicles, which could be detected by the reflected signals produced on the installed surface-wave structure.

Manuscript received November 13, 1973; revised July 15, 1974. This work was supported by the Canadian Institute of Guided Ground Transport, Queen's University, Kingston, Ont., Canada.

S. F. Mahmoud was with the Department of Electrical Engineering, Queen's University, Kingston, Ont., Canada. He is now with the Department of Electrical Engineering, Cairo University, Cairo, Egypt.

J. C. Beal is with the Department of Electrical Engineering, Queen's University, Kingston, Ont., Canada.

In this paper we present a theoretical approach to the problem of a metallic obstacle close to a surface-wave transmission line and derive expressions for the reflection and transmission coefficients, and the radiated power. The only previous detailed work on this subject appears to be that by Gillespie and Gustincic [5], [15] and Gillespie [6], for the Goubau line and a planar line, while Duncan and DuHamel [7] have reported some experimental measurements on obstacles near a dielectric-image line, in which the ultimate aim was the radically different one of influencing the radiation pattern of surface-wave antennas.

We concentrate here on the dielectric-image line which is taken as a convenient representative of a wide range of possible practical guiding structures. Similarly, we concentrate on highly idealized obstacles consisting of thin plane metallic sheets which yet can be considered to give a useful approximation to the reflection coefficient produced by a preceding vehicle. The approach used here consists of the expansion of the total field on the line in terms of a complete set of eigenmodes which include both the discrete and continuous spectra. The method is applicable to any line for which this complete set of eigenmodes is known or can be derived.

The theoretical steps followed to obtain the surface-wave reflection coefficient are as follows.

1) A complete set of orthogonal eigenmodes is obtained for the dielectric-image line. This includes both a discrete and a continuous spectrum of modes.

2) The fields excited by an arbitrary source are derived in terms of the above set of eigenmodes. The Green's dyad, defined later, is constructed from these fields.

3) An integral equation for the unknown current distribution on the obstacle surface is obtained in terms of the Green's dyad. A numerical solution of this equation for the current leads to the derivation of reflection and transmission coefficients of the surface wave.

II. MODE SPECTRA OF THE DIELECTRIC-IMAGE LINE

It is known that the eigenmodes of any open waveguide contain both discrete and continuous spectra. Any single mode of these spectra satisfies the source-free Maxwell's equations and the appropriate boundary conditions of the structure. It is important to notice that if the radiation condition is enforced at infinite distances from the waveguide, only the discrete modes (or surface-wave modes) can be obtained [8, chap. 1]. In order to find the complete set of eigenmodes, the radiation condition should not be

enforced. This fact has been realized by Shevchenko [8] who replaced the radiation condition by a less stringent one that requires only the finiteness of the fields at infinity. Using this approach, he has indicated a method of deriving the complete set of eigenmodes for an open structure. We apply this method here to the dielectric-image line and obtain both the discrete (surface-wave) and the continuous eigenmodes. It is worth mentioning that Snyder [9] has dealt with the problem in connection with the dielectric rod, where the author identifies the continuous modes with the fields of a scattered incident plane wave of which a prior knowledge is available. The present formulation is an alternative one which does not require such a knowledge.

The fields on the dielectric-image line can be expressed in terms of the scalar longitudinal electric and magnetic fields, e_z and h_z, which in turn satisfy the Helmholtz equation. We seek a solution characterized by a transverse wavenumber κ in the air region, with an mth harmonic in the ϕ direction [Fig. 1(a)]. Hence, apart from a common factor $\exp(-j\beta z)$, we write for the fields:

$$\begin{aligned} e_z(\rho,\phi) &= AJ_m(S\rho)\sin m\phi \\ h_z(\rho,\phi) &= BJ_m(S\rho)\cos m\phi, \qquad \text{for } 0 \leq \rho \leq \rho_0 \end{aligned} \tag{1a}$$

and

$$\begin{aligned} e_z(\rho,\phi) &= [V_e H_m^{(2)}(\kappa\rho) + W_e H_m^{(1)}(\kappa\rho)]\sin m\phi \\ h_z(\rho,\phi) &= [V_h H_m^{(2)}(\kappa\rho) + W_h H_m^{(1)}(\kappa\rho)]\cos m\phi, \\ &\qquad \text{for } \rho \geq \rho_0. \end{aligned} \tag{1b}$$

It should be noted that (1) applies to both discrete and continuous mode spectra as will be seen later in this section.

A, B, V_e, W_e, V_h, and W_h are constants for a given κ. The wavenumbers S and β are given by

$$\begin{aligned} \beta(\kappa) &= (1 - \kappa^2)^{1/2} \\ S(\kappa) &= (\epsilon_r - 1 - \kappa^2)^{1/2} \end{aligned}$$

where ϵ_r is the relative permittivity of the dielectric. Notice that all wavenumbers are normalized with respect to that of free space k_0. Consequently, all lengths will be normalized with respect to $1/k_0$. In addition, we shall normalize impedances with respect to 120π, the free-space plane wave impedance.

The transverse fields can be obtained from the longitudinal components through well-known formulas (see Appendix I). The continuity of e_z, e_ϕ, h_z, and h_ϕ provides four equations relating the six constants A, B, V_e, W_e, V_h, and W_h. The last four can then be expressed in terms of A and B as follows:

$$\begin{aligned} V_e &= a(\kappa)A + b(\kappa)B \\ W_e &= c(\kappa)A + d(\kappa)B \\ V_h &= b(\kappa)A + e(\kappa)B \\ W_h &= d(\kappa)A + f(\kappa)B \end{aligned} \tag{2}$$

where the quantities a, b, c, d, e, and f are given by [4]

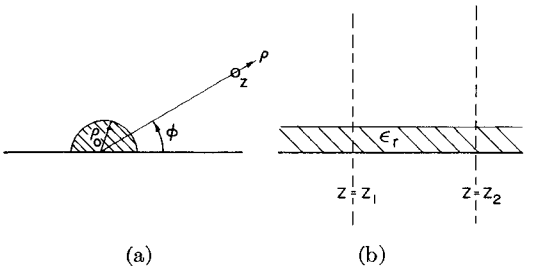

(a) (b)

Fig. 1. The dielectric-image line.

$$a(\kappa) = \frac{J_m(S\rho_0)H_m'^{(1)}(\kappa\rho_0) - (\epsilon_r\kappa/S)J_m'(S\rho_0)H_m^{(1)}(\kappa\rho_0)}{D}$$

$$b(\kappa) = -\frac{m\beta}{\kappa\rho_0}\frac{\epsilon_r - 1}{S^2}J_m(S\rho_0)H_m^{(1)}(\kappa\rho_0)/D$$

$$c(\kappa) = -\frac{J_m(S\rho_0)H_m'^{(2)}(\kappa\rho_0) - (\epsilon_r\kappa/S)J_m'(S\rho_0)H_m^{(2)}(\kappa\rho_0)}{D}$$

$$d(\kappa) = \frac{m\beta}{\kappa\rho_0}\frac{\epsilon_r - 1}{S^2}J_m(S\rho_0)H_m^{(2)}(\kappa\rho_0)/D \tag{3}$$

and $e(\kappa)$ and $f(\kappa)$ are the same as $a(\kappa)$ and $c(\kappa)$, respectively, but with the term ϵ_r in the latter expressions replaced by unity. The prime on the Bessel functions J_m and H_m denotes differentiation with respect to the argument. D is the Wronskian of the Hankel functions $H_m^{(1)}$ and $H_m^{(2)}$ and is given by

$$\begin{aligned} D(\kappa) &= H_m'^{(1)}(\kappa\rho_0)H_m^{(2)}(\kappa\rho_0) - H_m^{(1)}(\kappa\rho_0)H_m'^{(2)}(\kappa\rho_0) \\ &= 4j/\pi\kappa\rho_0. \end{aligned}$$

A. The Discrete Spectrum

The radiation condition states that [10]

$$\lim_{r\to\infty} r^{1/2}(\partial\psi/\partial r + jk_0\psi) \to 0 \tag{4}$$

where $r = (\rho^2 + z^2)^{1/2}$ and ψ is any scalar field quantity. This means that the field should decay in the far zone as fast, or faster than, a diverging spherical wave. If the fields e_z and h_z in (2) are to satisfy the radiation condition (4), then we should have

$$W_e(\kappa) = W_h(\kappa) = 0 \quad \text{with} \quad \text{Im}(\kappa) < 0 \tag{5}$$

which leads to fields that are evanescent in the transverse direction. These constitute the well-known surface-wave modes of the structure. Using (5) in (2), we obtain the dispersion equation for these modes as

$$c(\kappa)f(\kappa) = d^2(\kappa). \tag{6}$$

By use of (3), it can be easily verified that (6) is equivalent to that obtained by Elsasser [11] for surface-wave modes on the dielectric-image line.

B. The Continuous Spectrum

We notice that the radiation condition (4) cannot be satisfied by any modes other than those for which (5) is

valid. Hence, it is not possible to obtain the eigenmodes of the continuous spectrum while retaining that condition. Following Shevchenko [8], since the radiation condition is not a necessary one, we relax it into a less stringent one that requires only the finiteness of the field of an eigenmode at infinity. This is given by the following:

$$\lim_{\rho\to\infty} \rho^{1/2}\psi = \text{finite.} \tag{7}$$

Condition (7) is satisfied by any mode with a purely real value of the transverse wavenumber κ [see (1b)]. These modes, which may be termed "pseudomodes" [8], constitute the continuous spectrum of the structure and their fields extend to infinity, but remain finite, in the transverse direction.

Since we have only four homogeneous equations with six unknowns in (2), some ratio, for instance B/A, is left free to assume any value while A or B may be assumed as unity. This suggests that there are basically two types of pseudomodes to be arbitrarily defined.

C. Orthogonality Consideration

Snyder [9] has defined the two types of pseudomodes by effectively choosing $W_e = 0$ and $W_h = 0$, respectively. Alternatively, we have found it convenient to use the following definition. Type "a" pseudomodes are characterized by $A = 1$ and $B = 0$, and type "b" pseudomodes are characterized by $B = 1$ and $A = r(\kappa)$, where $r(\kappa)$ is chosen such that these two types of modes are mutually orthogonal for any pair of transverse wavenumbers κ and κ'. The quantity $r(\kappa)$ is related to the coefficients $a(\kappa)$, $b(\kappa)\cdots$ of (3) as [4]

$$\begin{aligned} r &= -(bc + de)/(ac + bd) \\ &= -(ad + bf)/(ac + bd) \end{aligned} \tag{8}$$

where the independent variable κ has been omitted in (8) for convenience. Using the preceding definitions in (2) we obtain the coefficients V_e, W_e, V_h, and W_h as

$$V_e = a \quad W_e = c \quad V_h = b \quad \text{and} \quad W_h = d \tag{9a}$$

for type "a" pseudomodes and

$$\begin{aligned} V_e &= d(b^2 - ae)/(ac + bd) \\ W_e &= b(d^2 - cf)/(ac + bd) \\ V_h &= -V_e \cdot c/d \end{aligned}$$

and

$$W_h = -W_e \cdot a/b \tag{9b}$$

for type "b" pseudomodes where the independent variable κ has again been dropped. The following orthogonality relationship can be obtained in a straightforward, although elaborate, procedure (see Appendix II):

$$\int_A \boldsymbol{e}_r(\kappa) \times\times \boldsymbol{h}_r(\kappa') \cdot \boldsymbol{z} dA = N_r(\kappa)\delta(\kappa - \kappa')$$

with

$$N_r(\kappa) = \frac{2\pi\beta(\kappa)}{\kappa^3}[V_h W_h + V_e W_e]_r. \tag{10}$$

A is the transverse cross section and the subscript r refers to the type of pseudomodes involved ("a" or "b"). The implicit dependence of the fields on ρ and ϕ is to be understood. Also, the V's and W's are functions of κ.

D. Excitation by an Arbitrary Source Distribution

The fields $(\boldsymbol{E}, \boldsymbol{H})$ produced by a given distribution of electric and magnetic currents $(\boldsymbol{J}, \boldsymbol{M})$ which lie between the transverse planes $z = z_1$ and $z = z_2$ [Fig. 1(b)] can be expressed in terms of the complete set of modes of the line. It is significant to realize that the problem is now essentially the same as that of field excitation in closed waveguides, for which a complete set of discrete modes exists (e.g., [12,sec.5.6]). Thus the fields $(\boldsymbol{E},\boldsymbol{H})$ are expanded in terms of the eigenmodes of the line and the coefficient of excitation of each eigenmode is obtained by the application of the Lorentz reciprocity theorem, along with the mutual orthogonality relationships among these modes. The results are stated below.

$$\begin{aligned} (\boldsymbol{E},\boldsymbol{H}) = &\sum_n A_n^{\pm}(\boldsymbol{e}_n^{\pm},\boldsymbol{h}_n^{\pm}) \exp(\mp j\beta_n z) \\ &+ \sum_{r=a}^{b} \int_0^{\infty} d\kappa B_r^{\pm}(\kappa)(\boldsymbol{e}_r^{\pm}(\kappa), \boldsymbol{h}_r^{\pm}(\kappa)) \\ &\cdot \exp(\mp j\beta(\kappa)z) \end{aligned} \tag{11}$$

where the first summation is over the finite number of discrete modes. The $\pm$ superscript refers to the regions $z > z_2$ and $z < z_1$, respectively, with $z_2 > z_1$. The subscript r refers to type "a" or type "b" pseudomodes over which the integration is taken. The excitation coefficients $A_n^{\pm}$ and $B_r^{\pm}(\kappa)$ are given by

$$A_n^{\pm} = \int_V (\boldsymbol{J}\cdot\boldsymbol{E}_n^{\mp} + \boldsymbol{M}\cdot\boldsymbol{H}_n^{\mp})\, dV/2N_n \tag{12a}$$

and

$$B_r^{\pm}(\kappa) = \int_V (\boldsymbol{J}\cdot\boldsymbol{E}_r^{\mp}(\kappa) + \boldsymbol{M}\cdot\boldsymbol{H}_r^{\mp}(\kappa))\, dV/2N_r(\kappa) \tag{12b}$$

where $\boldsymbol{E}_r^{\pm}(\kappa) = \boldsymbol{e}_r^{\pm}(\kappa) \exp(\mp j\beta(\kappa)z)$, and similar interpretations exist for $\boldsymbol{H}_r^{\pm}(\kappa)$, $\boldsymbol{E}_n^{\pm}$, and $\boldsymbol{H}_n^{\pm}$.

The normalization factor $N_r(\kappa)$ is defined in (10) and N_n is the corresponding quantity for the nth discrete mode.

III. THE SEMIANNULAR METALLIC OBSTACLE

A. Formulation

The geometry of the problem is shown in Fig. 2. The incident wave on the line is the dominant HE_{11} mode which is assumed to be the only surface-wave mode supported by the line. As the face of the obstacle fits the coordinate system and extends fully over the range of ϕ ($0 \le \phi \le \pi$), the scattered fields are expected to have the same dependence on ϕ as the incident fields, i.e., a $\sin\phi$ or $\cos\phi$ variation. Hence, in the subsequent analysis, the ϕ dependence of the fields can be omitted.

The method of solution adopted here is to form an

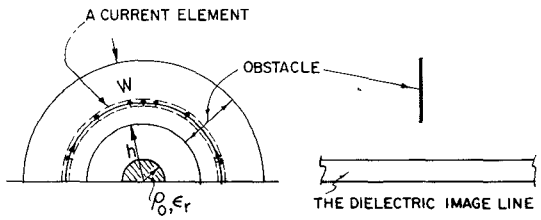

Fig. 2. Semiannular obstacle above the dielectric-image line.

equivalent problem where the obstacle is replaced by an electric current sheet that lies on the closed boundary surface S of the obstacle. This current sheet, so far unknown, is determined such that the total tangential electric field (incident plus scattered due to the current sheet) at the surface S is equal to zero. This method can be applied, in principle, to any obstacle of arbitrary shape, such as a thick perfectly conducting sheet. However, the numerical solution of the resulting equations will be extremely complicated. Hence, we shall concentrate on a very thin obstacle such as that of Fig. 2 which we can replace, in the limit of infinitesimal thickness, by a single current sheet of electric current in the plane $z = 0$. This current will satisfy the edge conditions, i.e., a zero normal current at the edges. Since the obstacle is assumed to have an infinitesimally small thickness, the boundary conditions requiring zero tangential electric fields at both sides of the obstacle reduce, in the limit, to the single boundary condition of the vanishing of that field only in the plane $z = 0$ and over the current sheet.

Let us assume that a Green's dyad operator $\mathsf{G}(\rho,\rho',z)$ can be found that relates the scattered electric field $\boldsymbol{E}_s$ to the equivalent current sheet $\boldsymbol{J}$ as follows:

$$\boldsymbol{E}_s(\rho,z) = \int_A \mathsf{G}(\rho,\rho',z)\cdot\boldsymbol{J}(\rho')\,dA$$

$$= \pi/2\int_{\rho'} \rho'\mathsf{G}(\rho,\rho',z)\cdot\boldsymbol{J}(\rho')\,d\rho' \qquad (13)$$

where the factor $\pi/2$ arises from an implicit integration over ϕ of $\sin^2\phi$ or $\cos^2\phi$. The range of ρ' is over the obstacle surface. The Green's dyad operator defined by (13) is seen to be different from the conventional Green's dyad function, such as that used by Collin [12,p.198], but it has the merit that it can be constructed directly from (11) and (12), when specialized to the case of impulsive sources. Now let $\boldsymbol{J}(\rho')$ be expressed in the following form:

$$\boldsymbol{J}(\rho') \triangleq [I_\rho(\rho')\boldsymbol{\rho} + I_\phi(\rho')\boldsymbol{\phi}]/(\pi\rho'/2)$$
$$\equiv \boldsymbol{I}(\rho')/(\pi\rho'/2)$$

where $\boldsymbol{I}$ has the dimensions of an ampere. When the preceding equation is substituted in (13) we get $\boldsymbol{E}_s(\rho,z)$ in the simple form

$$\boldsymbol{E}_s(\rho,z) = \int_{\rho'} \mathsf{G}(\rho,\rho',z)\cdot\boldsymbol{I}(\rho')d\rho'.$$

From this point onwards, we shall drop the longitudinal components of G and hence retain only the transverse components. The vanishing of the total tangential electric field on the metallic obstacle reduces to

$$\int \mathsf{G}(\rho,\rho')\cdot\boldsymbol{I}(\rho')\,d\rho' = -\boldsymbol{e}_{\text{inc}}(\rho) \qquad (14)$$

where both ρ and ρ' lie on the obstacle surface. It is understood that z is set equal to zero since the fields are at the obstacle surface.

To solve (14) for the unknown current distribution $\boldsymbol{I}(\rho')$ we expand this into a summation of a complete set of vector functions $f_i(\rho')$, $i = 1,2,\cdots$, each of which satisfies the edge condition that the radial current is zero at $\rho' = h$ and $h + W$; a suitable set of sine and cosine functions was used in the computation. Thus we have

$$\boldsymbol{I}(\rho') = \sum_i a_i\boldsymbol{f}_i(\rho'). \qquad (15)$$

Substituting in (14) we get

$$\sum_i a_i\int \mathsf{G}(\rho,\rho')\cdot\boldsymbol{f}_i(\rho')d\rho' = -\boldsymbol{e}_{\text{inc}}(\rho). \qquad (16)$$

To obtain the coefficients a_i, $i = 1,2,\cdots$, we scalar multiply (16) by a complete set of vector test functions and integrate over ρ. If we choose the same set of functions that have been used for the current distribution, we end up with the following system of linear equations:

$$\sum_i a_i\int \langle \boldsymbol{f}_j(\rho), \mathsf{G}(\rho,\rho')\cdot\boldsymbol{f}_i(\rho)\rangle\,d\rho'$$
$$= -\langle \boldsymbol{f}_j(\rho), \boldsymbol{e}_{\text{inc}}(\rho)\rangle, \qquad j = 1,2,\cdots \qquad (17)$$

where, in general terms,

$$\langle \boldsymbol{a}(\rho), \boldsymbol{b}(\rho)\rangle \triangleq \int_h^{h+w} \boldsymbol{a}(\rho)\cdot\boldsymbol{b}(\rho)d\rho.$$

This system of equations is infinite. However, we truncate the sum in (15) at a suitable number of terms N, and the finite system of equations thus obtained can be solved numerically to yield the coefficients a_i, $i = 1,2,\cdots,N$, and hence the current distribution. The surface-wave reflection coefficient is given as

$$R = -\tfrac{1}{2}\langle \boldsymbol{I}(\rho), \boldsymbol{e}_{\text{inc}}(\rho)\rangle$$
$$= -\tfrac{1}{2}\sum_i a_i\langle \boldsymbol{f}_i(\rho), \boldsymbol{e}_{\text{inc}}(\rho)\rangle \qquad (18)$$

by virtue of (12a) and the assumption that $\boldsymbol{e}_{\text{inc}}(\rho)$, which is the incident electric field, is normalized such that

$$N_{\text{inc}} \equiv \tfrac{1}{2}\pi\int_0^\infty \boldsymbol{e}_{\text{inc}}(\rho)\times\boldsymbol{h}_{\text{inc}}(\rho)\rho\,d\rho = 1.$$

It is important to notice that expression (18) for R is, in effect, a stationary one with respect to the current distribution under the conditions given by (17). This can be easily verified by use of the Rayleigh–Ritz method [12] to show that the preceding conditions are exactly the same

as those that render the following expression for R a stationary one:

$$R = \tfrac{1}{2}\langle \boldsymbol{I}(\rho), \boldsymbol{e}_{inc}(\rho)\rangle^2 / \langle \boldsymbol{I}(\rho), \boldsymbol{E}_s(\rho)\rangle \tag{19}$$

where $\boldsymbol{E}_s(\rho)$ is the scattered electric field by the assumed current distribution.

B. The Green's Dyad $\mathsf{G}(\rho,\rho')$

The Green's dyad $\mathsf{G}(\rho,\rho')$ is obtained from the transverse electric field given by (11) and (12) under the special case where $z_1 = z_2 = 0$, $\boldsymbol{M} = 0$, and J is a unit source given by

$$J(\rho') = J_\rho \boldsymbol{\rho} + J_\phi \boldsymbol{\phi}$$

with

$$J_\rho = J_\phi = \delta(\rho - \rho')\delta(z)/(\pi\rho'/2). \tag{20}$$

Upon substituting in (11) and (12), we obtain

$$\mathsf{G}(\rho,\rho') = \sum_i \frac{1}{2N_i} \boldsymbol{e}_i(\rho)\boldsymbol{e}_i(\rho') + \sum_{r=a}^{b} \int_0^\infty \frac{d\kappa}{2N_r(\kappa)} \boldsymbol{e}_r(\rho,\kappa)\boldsymbol{e}_r(\rho',\kappa) \tag{21}$$

where $\boldsymbol{e}_i(\rho)$ and $\boldsymbol{e}_r(\rho,\kappa)$ are the transverse electric field of the discrete and continuous spectra, respectively. The second summation is over the two types of pseudomodes. In a matrix form, the Green's dyad has four elements, namely, $G_{\rho\rho}$, $G_{\rho\phi}$, $G_{\phi\rho}$, and $G_{\phi\phi}$, where, for example, $G_{\rho\phi}$ denotes the radial electric field produced by a unit circumferentially directed $\boldsymbol{I}$ source and is therefore given explicitly by

$$G_{\rho\phi}(\rho,\rho') = \sum_i e_{i\rho}(\rho)e_{i\phi}(\rho')/2N_i + \sum_r \int_0^\infty d\kappa e_{r\rho}(\rho,\kappa)e_{r\phi}(\rho',\kappa)/2N_r(\kappa). \tag{22}$$

For a practical line, the number of discrete modes is just one—the dominant mode. For a given source point ρ' and a field point ρ, the discrete sum in (21) is straightforward to evaluate. The continuous sum needs to be evaluated by integration. However, in its present form, the integrand is oscillating too rapidly with κ to allow for an accurate integration. We therefore change the integration path into another path in the complex κ plane. At this point, we should notice that (21) contains eight integrations to be performed for the four scalar components of the Green's dyad. Any of these integrations can be cast into the form

$$\int_0^\infty d\kappa (F_u(\kappa) + F_L(\kappa)) \tag{23}$$

where $F_u(\kappa)$ is analytic in the upper half-plane of κ and $F_L(\kappa)$ is analytic in the lower half of the plane. A relation exists between $F_u(\kappa)$ and $F_L(\kappa)$ which is

$$F_u^*(\kappa) = -F_L(\kappa^*). \tag{24}$$

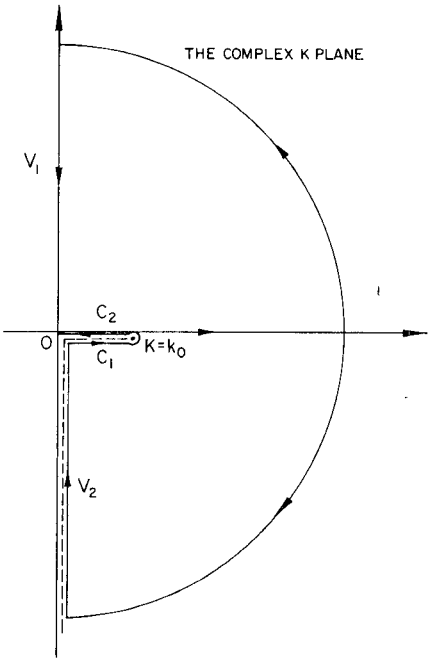

Fig. 3 Change of integration path in the complex κ plane.

Hence, the integrand in (22) is completely determined by $F_u(\kappa)$ alone for which expressions are displayed in Appendix III. The change of the path of integration in (23) is performed according to Fig. 3. For $F_u(\kappa)$ we close the contour in the upper half-plane and for $F_L(\kappa)$, we close it in the lower half-plane. Due to the branch point at $\kappa = 1$, the contributions of $F_L(\kappa)$ on C_1 and C_2 paths add up in phase. It is then easy to show that the integration in (23) reduces to

$$\int_{-V_1} F_u(\kappa)\, d\kappa + \int_{-V_2} F_L(\kappa)\, d\kappa - 2\int_{C_1} F_L(\kappa)\, d\kappa = \int_{-V_1} [F_u(\kappa) - F_u^*(\kappa)]\, d\kappa + 2\int_0^1 F_u(\kappa)\, d\kappa. \tag{25}$$

Poles encircled by the contours belong to leaky modes; i.e., they lie on the improper side of the branch cut, and hence their residues are not included in (25). Moreover, the surface-wave pole on the vertical axis has a zero residue and hence zero contribution. Now, the integrand on V_1 does not oscillate rapidly with (κ), and hence an accurate numerical integration can be performed.

IV. NUMERICAL COMPUTATION AND RESULTS

As stated earlier, the surface-wave reflection coefficient R is obtained by first solving the truncated system of linear equations (17) and then using the result in (18). The inner products in (17) were computed by dividing the obstacle surface radially into a finite number of segments and the Green's function over each was assumed constant. A radial length of $\lambda_0/60$ for each segment proved to result in an adequate accuracy. The singularity that arises in calculating $\mathsf{G}(\rho,\rho)$ was resolved by assuming that the ob-

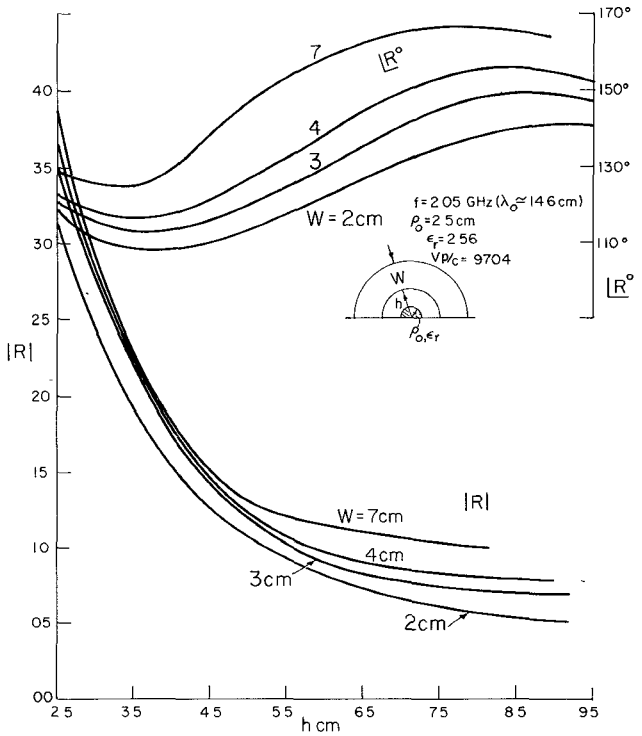

Fig. 4. Surface-wave reflection coefficient, magnitude, and phase.

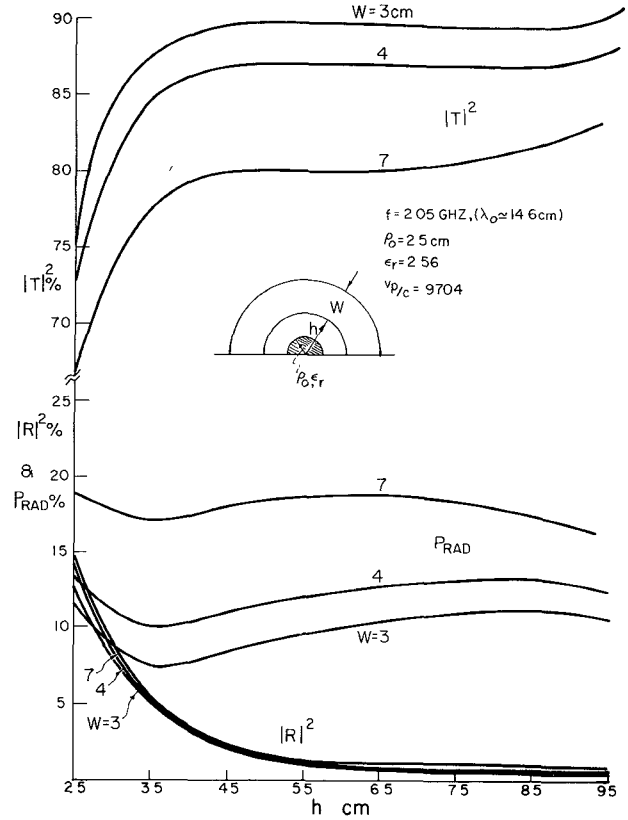

Fig. 5. Reflected, transmitted, and radiated powers.

servation point has a z coordinate dz, integrating the fields over the segment, and then putting $dz \rightarrow 0$ [4]. The number of the equations N in (17) was increased until a clear convergence of R was noticed. Three to five harmonics of the current ($N = 3 \rightarrow 5$) have been found sufficient to produce a convergence in R. The surface-wave transmission coefficient T is given by

$$T = 1 + R. \tag{26}$$

This follows directly from matching of the surface-wave components of the tangential electric field on both sides of this idealized obstacle [6]. The transmitted surface-wave power, normalized to a unit incident power, is then given by $| T |^2$ and the radiated power P_{rad} is obtained such that the power balance equation is satisfied, i.e.,

$$P_{\text{rad}} + | R |^2 + | T |^2 = 1. \tag{27}$$

Fig. 4 shows magnitudes and phases of the surface-wave reflection coefficient for various obstacles of height h and width W. The surface-wave phase velocity is fixed at 97.04 percent of the free-space velocity. Wavelengths correspond to a frequency of 2.05 GHz, but all lengths involved can be scaled up or down according to the applied frequency. The percentages of surface-wave power reflected, transmitted, as well as the power radiated by the obstacle, are shown in Fig. 5.

The following remarks apply to Figs. 4 and 5.

1) The magnitude of the reflection coefficient decays with an increase of h. The phase tends to oscillate with h but the wider the obstacle the closer is the phase to π radians. This can be compared with the extreme case when the obstacle covers the whole $z = 0$ half-plane and the phase of R becomes exactly π radians.

2) We notice that the radiated power P_{rad} is generally greater than the surface-wave reflected power $| R |^2$ and is likely to be always a significant fraction of the total scattered power. This fact has also been reported by Gillespie [6], in relation to rings around the Goubau line, and experimentally observed on the dielectric-image line by Duncan and DuHamel [7]. The relatively low values of surface-wave reflection coefficients may set a limitation on the sensitivity of obstacle detection schemes for ground transportation. Nevertheless, this can be overcome by the use of repeaters along the guide-way to enhance the reflected signals [2].

3) The radiated power, plotted versus obstacle height, tends to have a flat peak associated with a corresponding minimum for the transmitted power $| T |^2$ (Fig. 5). The value of h at which this peak and minimum occur is less for larger obstacle widths. It is interesting to notice that the same phenomenon occurs in a more pronounced form in the results of Gillespie and Kilburg [13], in relation to the scattering from a conducting strip above a plane surface-wave guide.

V. CONCLUSIONS

A theoretical approach has been described to the study of reflections from metallic obstacles in the vicinity of dielectric-image lines. The main feature of the method is the use of the concept of the complete set of eigenmodes of the guiding structure, which enables both the scattered surface-wave modes and the radiation to be derived from the same initial formulation of the problem. Results have been presented for the particular case of a very thin

metallic annulus placed symmetrically about a dielectric-image line, but the method is readily adaptable to metallic obstacles of a more general nature by an extended use of the numerical techniques applied here. Similarly, the dielectric-image line has been used as a surface-wave transmission line representative of a wide range of possible guiding structures more appropriate to practical installations, to which this same method can be applied.

This work has been motivated by the need to develop more refined obstacle detection schemes for use in high-speed railways, automated highways, and other ground transportation systems of the near future.

APPENDIX I

TRANSVERSE FIELDS

The transverse fields $\boldsymbol{e}_t$ and $\boldsymbol{h}_t$ are derived from the longitudinal fields $\boldsymbol{e}_z$ and $\boldsymbol{h}_z$ through the formulas (e.g., [14])

$$\boldsymbol{e}_t = \frac{j\beta}{\epsilon_r - \beta^2}\left[\nabla_t e_z + \frac{1}{\beta}\boldsymbol{z} \times \nabla_t h_z\right] \tag{A.1}$$

$$\boldsymbol{h}_t = \frac{j\beta}{\epsilon_r - \beta^2}\left[-\nabla_t h_z - \frac{\epsilon_r}{\beta}\boldsymbol{z} \times \nabla_t e_z\right] \tag{A.2}$$

where ∇_t is the transverse gradient operator. The two preceding equations apply for $\rho \leq \rho_0$, i.e., inside the dielectric rod. For $\rho > \rho_0$, ϵ_r should be replaced by unity.

APPENDIX II

PROOF OF THE ORTHOGONALITY RELATIONSHIP (10)

Let us assume that the vector fields of two pseudomodes are given by

$$(\boldsymbol{e}(\kappa), \boldsymbol{h}(\kappa)) \exp(-j\beta z)$$

and

$$(\boldsymbol{e}(\kappa'), \boldsymbol{h}(\kappa')) \exp(-j\beta' z)$$

where $\boldsymbol{e}(\kappa), \boldsymbol{h}(\kappa), \cdots$ are functions of the transverse coordinates only, $\beta = (1 - \kappa^2)^{1/2}$, $\beta' = (1 - \kappa'^2)^{1/2}$, and κ and κ' are the respective normalized transverse wavenumbers. It is a routine matter to derive the following relationship among the above fields (see, e.g., [16]):

$$\int_A [\boldsymbol{e}(\kappa) \times \boldsymbol{h}(\kappa') - \boldsymbol{e}(\kappa') \times \boldsymbol{h}(\kappa)] \cdot \boldsymbol{z}\, dA$$

$$= \frac{1}{j(\beta + \beta')} \oint_C [\boldsymbol{e}(\kappa) \times \boldsymbol{h}(\kappa') - \boldsymbol{e}(\kappa') \times \boldsymbol{h}(\kappa)] \cdot \boldsymbol{n}\, dl \tag{A.3}$$

where A is the transverse cross-sectional area over which the fields are defined, C is a closed line contour that encloses A, and $\boldsymbol{n}$ is the outward normal to C. For the dielectric-image line (Fig. 1) C consists of a semicircle $\rho = R \to \infty$, $0 \leq \varphi \leq \pi$ taken in an anticlockwise direction and a line closing it that lies totally on the conductive plane. Obviously the integration over this line is zero, and we are left with an integration over the infinitely large semicircle. For modes which satisfy the radiation condition (4), this integration is also zero, and the orthogonality relationship is already proved. However, for pseudomodes which satisfy (7) instead, this is not obvious, and that integration needs to be evaluated. We proceed to do so.

For $\kappa\rho = \kappa R \to \infty$, the following asymptotic formulas for the field components are obtained by use of (1b), (A.1), and (A.2):

$$(e_z, h_z) \to [(V_e, V_h) \exp(-j\kappa R + j\alpha) + (W_e, W_h) \cdot \exp(j\kappa R - j\alpha)](2/\pi\kappa R)^{1/2} \cdot (\sin, \cos) m\varphi$$

$$(e_\varphi, h_\varphi) = [(V_h, -V_e) \exp(-j\kappa R + j\alpha) - (W_h, -W_e) \cdot \exp(j\kappa R - j\alpha)](2/\pi\kappa^3 R)^{1/2} \cdot (\cos, \sin) m\varphi \tag{A.4}$$

where $\alpha = m\pi/2 + \pi/4$. In (A.4) we have substituted for the Hankel functions by the first term in their asymptotic expansion. The field components in (A.4) are those needed in the right-hand side (RHS) of (A.3). If the two pseudomodes have the same value of m, the integration over φ is nonzero, and the RHS of (A.3) becomes

RHS of (A.3)

$$= \frac{\pi/2}{j(\beta + \beta')} \lim_{R \to \infty} R[(e_\varphi h_z' - e_\varphi' h_z) - (e_z h_\varphi' - e_z' h_\varphi)] \tag{A.5}$$

where e_z is the z component of $\boldsymbol{e}(\kappa)$ e_z' is the z component of $\boldsymbol{e}(\kappa')$, and so forth.

Now we substitute from (A.4) in (A.5) and after some algebra we obtain:

RHS of (A.3)

$$= \frac{(\kappa\kappa')^{-3/2}}{j(\beta + \beta')} \cdot (\kappa^2 - \kappa'^2) \cdot \lim_{R \to \infty} [L_R(\kappa, \kappa')] \tag{A.6}$$

where

$$\begin{aligned} L_R(\kappa,\kappa') = {} & \frac{\cos[(\kappa + \kappa')R - 2\alpha]}{\kappa + \kappa'} \cdot (W_h W_h' - W_e W_e' - V_h V_h' + V_e V_e') \\ & + j\frac{\sin[(\kappa + \kappa')R - 2\alpha]}{\kappa + \kappa'} \cdot (W_h W_h' - W_e W_e' + V_h V_h' - V_e V_e') \\ & + \frac{\cos[(\kappa - \kappa')R]}{\kappa - \kappa'} \cdot (V_h W_h' - V_e W_e' + V_e' W_e - V_h' W_h) \\ & + j\frac{\sin[(\kappa - \kappa')R]}{\kappa - \kappa'} \cdot (V_e' W_e + V_e W_e' - V_h' W_h - V_h W_h'). \end{aligned} \tag{A.7}$$

It is constructive to notice the similarity between (A.7) and [8, eq.17.8]. The only surviving term in (A.7) as $R \to \infty$ is the last one. So

$$\lim_{R\to\infty} L_R(\kappa,\kappa') \to j\pi\delta(\kappa - \kappa') \cdot (V_e'W_e + V_eW_e' - V_h'W_h - V_hW_h'). \quad \text{(A.8)}$$

As $\kappa \to \kappa'$, we assume that $\beta' \to -\beta$ so that the quantity $(\kappa^2 - \kappa'^2)/(\beta + \beta') \to -2\beta$. Now, substituting this result and (A.8) in (A.6) we obtain

$$\text{RHS OF (A.3)} = \frac{4\pi\beta}{\kappa^3}[V_hW_h + V_eW_h]. \quad \text{(A.9)}$$

To obtain (A.9) we have substituted for V_e', W_e', V_h', and W_h' by V_e, W_e, $-V_h$, and $-W_h$, respectively, since V_e and W_e are even functions of β, while V_h and W_h are odd functions of β (or at least, this is a consistent assumption; see (2) and (3) in the text).

Equation (10) in the text is obtained directly from a combination of (A.3) and (A.9).

APPENDIX III

EXPRESSIONS FOR $F_u(\kappa)$ IN (23)

The Green's dyad has four scalar components, namely, $G_{\rho\rho}$, $G_{\varphi\rho}$, $G_{\rho\varphi}$, and $G_{\varphi\varphi}$. To each there are associated two expressions for $F_u(\kappa)$ corresponding to the "a" and "b" type pseudomodes. Expressions of $F_u(\kappa)$ are obtained from combinations of (21), (23), and (A.1). Thus we have

$$F_u^{\rho\rho}(\kappa) = \frac{\beta(\kappa)\kappa}{4\pi N(\kappa)} X_1(\rho)\{X_1(\rho') + X_2(\rho')\}$$

$$F_u^{\varphi\rho}(\kappa) = \frac{\kappa}{4\pi N(\kappa)} Y_1(\rho)\{X_1(\rho') + X_2(\rho')\}$$

$$F_u^{\rho\varphi}(\kappa) = \frac{\kappa}{4\pi N(\kappa)} X_1(\rho)\{Y_1(\rho') + Y_2(\rho')\}$$

and

$$F_u^{\varphi\varphi}(\kappa) = \frac{-\kappa}{4\pi\beta(\kappa)N(\kappa)} Y_1(\rho)\{Y_1(\rho') + Y_2(\rho')\} \quad \text{(A.10)}$$

where

$$X_1(\rho) = W_eH_1'^{(1)}(\kappa\rho) - W_hH_1^{(1)}(\kappa\rho)/\kappa\beta(\kappa)\rho$$

$$X_2(\rho) = V_eH_1'^{(2)}(\kappa\rho) - V_hH_1^{(2)}(\kappa\rho)/\kappa\beta(\kappa)\rho$$

$$Y_1(\rho) = W_hH_1'^{(1)}(\kappa\rho) - \beta(\kappa)W_eH_1^{(1)}(\kappa\rho)/\kappa\rho$$

and

$$Y_2(\rho) = V_hH_1'^{(2)}(\kappa\rho) - \beta(\kappa)V_eH_1^{(2)}(\kappa\rho)/\kappa\rho. \quad \text{(A.11)}$$

We notice that the coefficients V_e, V_h, W_e, and W_h are functions of κ. The preceding expressions for $F_u(\kappa)$ belong to "a" or "b" pseudomodes according to whether the coefficients V_e, V_h, W_e, and W_h belong to "a" or "b" pseudomodes. These are given by (9a) and (9b) in the text.

REFERENCES

[1] R. L. Gallawa *et al.*, "The surface-wave transmission line and its use in communicating with high-speed vehicles," *IEEE Trans. Commun. Technol.*, vol. COM-17, pp. 518–525, Oct. 1969.

[2] J. C. Beal, J. Josiak, S. F. Mahmoud, and V. Rawat, "Continuous access guided communication (CAGC) for ground-transportation systems," *Proc. IEEE (Special Issue on Ground Transportation for the Eighties)*, vol. 61, pp. 562–568, May 1973.

[3] L. M. Smith, "Guided radar for obstacle detection," M.Sc. thesis, Queen's Univ., Kingston, Ont., Canada, 1973.

[4] S. F. Mahmoud, "Electromagnetic aspects of guided radar for guided ground transportation," Ph.D. dissertation, Queen's Univ., Kingston, Ont., Canada, 1973.

[5] E. S. Gillespie and J. J. Gustincic, "The scattering of an axial cylindrical surface wave by a perfectly conducting plane annulus," *IEEE Trans. Microwave Theory Tech.*, vol. MTT-16, pp. 334–341, June 1968.

[6] E. S. Gillespie, "The impedance and scattering properties of a plane annulus surrounding a Goubau line," *IEEE Trans. Microwave Theory Tech.* (Corresp.), vol. MTT-19, pp. 837–838, Oct. 1971.

[7] J. W. Duncan and R. H. DuHamel, "A technique in controlling the radiation from dielectric rod waveguides," *IEEE Trans. Antennas Propagat.*, vol. AP-5, pp. 284–289, July 1957.

[8] V. V. Shevchenko, *Continuous Transitions in Open Waveguides*, P. Beckman, Transl. Boulder, Colo.: Golem, 1971.

[9] A. W. Snyder, "Continuous mode spectrum of a circular dielectric rod," *IEEE Trans. Microwave Theory Tech.*, vol. MTT-19, pp. 720–727, Aug. 1971.

[10] D. S. Jones, *The Theory of Electromagnetism*. New York: Pergamon, 1964, sec. 1.27.

[11] W. M. Elsasser, "Attenuation in a dielectric circular rod," *J. Appl. Phys.*, vol. 20, pp. 1193–1196, Dec. 1949.

[12] R. E. Collin, *Field Theory of Guided Waves*. New York: McGraw-Hill, 1960.

[13] E. S. Gillespie and F. J. Kilburg, "The impedance scattering properties of a perfectly conducting strip above a plane surface-wave system," *IEEE Trans. Microwave Theory Tech.* (Short Papers), vol. MTT-21, pp. 413–419, June 1973.

[14] Y. Garault, "Hybrid EG guided waves," in *Advances in Microwaves*, vol. 5, L. Young, Ed. New York: Academic, 1970, pp. 188–306.

[15] E. S. Gillespie and J. J. Gustincic. "The scattering of a TM surface wave by a perfectly conducting strip," *IEEE Trans. Microwave Theory Tech.* (*Special Issue on Microwave Filters*), vol. MTT-13, pp. 630–640, Sept. 1965.

[16] L. R. Walker, "Orthogonality relations for gyrotropic waveguides," *J. Appl. Phys.*, vol. 28, p. 317, Mar. 1957.